Antioxidative Impact of Phenolics-Loaded Nanocarriers on Cytoskeletal Network Remodeling of Invasive Cancer Cells

Jaewon Jung,[#] Minhee Ku,[#] Suhui Jeong,[#] Nara Yoon, Jae Hyun Park, Han Sung Youn, Jaemoon Yang,* and Sungbaek Seo*

Cite This: https://doi.org/10.1021/acsami.3c04693

Read Online

ACCESS | Metrics & More | Article Recommendations | Supporting Information

ABSTRACT: Natural phenolic compounds have antioxidant properties owing to their free radical-scavenging capability. The combined effect of a mixture of phenolic compounds has been studied; however, the detailed investigation for finding a correlation between single phenolic molecules and antioxidant activity has not been explored. Herein, we revealed that the number of phenolic hydroxyl groups in phenolics played a central role in their antioxidant capacity. Based on the finding, tannic acid showed the most effective antioxidant potential, e.g., 76% in tannic acid versus 22% in vitamin C as a standard antioxidant component. Because cancer progression is closely related to oxidative processes at the cellular level, we further applied the surface treatment of tannic acid drug-delivery nanocarriers. Tannic acid-loaded nanocarriers reduced reactive oxygen species of cancer cells as much as 41% of vehicle treatment and remodeled cytoskeletal network. By a gelatin degradation study, TA-loaded nanocarrier-treated cells induced 44.6% reduction of degraded area than vehicle-treated cells, implying a potential of blocking invasiveness of cancer cells.

KEYWORDS: antioxidant, cancer cell, cytoskeletal network, invasive potential, phenolics
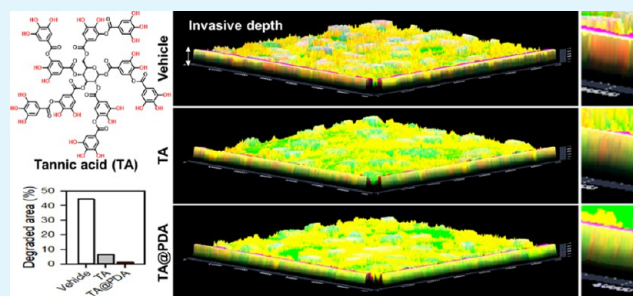
1. INTRODUCTION

Phenolic compounds are common phytochemicals found in plant tissues, such as fruits and vegetables. They possess various bioactive properties, particularly antioxidative properties, owing to their free radical-scavenging capability. For this reason, natural phenolic compounds have been utilized as anti-aging components or additives in cosmetics, dietary supplements, and pharmaceuticals.[1−3] For example, well-known natural phenolic compounds in medicinal herbs have been widely used as anti-aging and dietary supplements.[4,5] The antioxidant performance of plant and fruit extracts and their health benefits have been investigated with the contribution of natural phenolic compounds inside.[6] For instance, the resveratrol extract shows very high antioxidant activity and potential cardioprotective and anticarcinogenic effects.[7] In addition, berry seed meals were identified as a good source of phenolic compounds that can inhibit copper-induced low-density lipoprotein-cholesterol oxidation and DNA damage, indicating that phenolic compounds may prevent atherosclerosis, mutagenesis, and carcinogenesis.[8−10] However, because the extract is a mixture of several constituents, including phenolic molecules (phenolics), researchers could not isolate the particular effect of single phenolics from the combined effect of the mixture.

Free radicals are molecular species with unpaired electrons in atomic orbitals. They are highly reactive, unstable, and can damage essential biomolecules, such as DNA, proteins, carbohydrates, and lipids in nuclei and cell membranes of the human body.[11] Phenolics can scavenge free radicals or antioxidants by transferring the hydrogen atom of the phenolic ring to free radicals. Delocalized or activated radical phenolics have high chemical stability due to the benzene ring resonance effect. Therefore, biological damage or deleterious oxidative stress caused by the free radicals surrounding the cells can be reduced in the presence of phenolics. Rigoussen et al.[12] reported that the antioxidant efficiency of biophenolics is closely related to the number of mesomeric forms of the phenolic ring structures—the more mesomeric the forms, the more efficient the antioxidation. In addition, the antioxidant efficiency is linked to substituting the aromatic ring in ortho- and para-positions and their steric hindrance.[13,14] However, to the best of our knowledge, the systematic correlation between the molecular structure of single phenolics and antioxidant activity and their influence on cell behavior is not fully understood.

Numerous diseases, such as carcinogenesis, cardiovascular diseases, neurodegeneration, and skin deterioration, are related to oxidative stress, for example, harmful free radicals.[11,15] The free radicals continually cause cell damage in carcinogenesis and indirectly affect cell progression. For these reasons, antioxidation-functionalized or supplementary drug-delivery carriers have recently developed.[16−18] Yi *et al.* utilized tea polyphenols as a component to formulate drug-delivery nanoparticles for anticancer therapy. The nanoparticles provided strong antioxidative capability, 10 times higher than polydopamine (a widely studied polyphenolic molecule)-based nanoparticles. Correspondingly, the polyphenol-cooperated drug-delivery nanoparticles showed a tumor inhibition rate of approximately 70%, reducing tumor progression.

In our previous study, surface primers with a phenolic group (*i.e.*, catecholic) were primarily used for surface anchoring on stiff composite materials.[19] Herein, we investigate antioxidative performance of the surface primer (considered a phenolic derivative) compared with other analogue phenolics and observe its antioxidant effect on cell behavior. We first investigated the effect of the number of phenolic hydroxyl groups (−OH) on antioxidant activity. In the simple phenolic series—phenol (one −OH), catechol (two −OH), and pyrogallol (three −OH)—the antioxidant activity of the phenolic series was analyzed by several free radical-scavenging assays. The phenolics' oxidation/reduction potentials and oxidation kinetics in the presence of the strong oxidant $NaIO_4$ were compared using a cyclic voltammetry (CV) diagram and UV−vis absorption spectra, respectively.

Based on the finding of the most prominent antioxidative capability and external stimulus-resistant phenolics, tannic acid was applied for the surface treatment of nanoparticle-based drug delivery carriers. Because the treated phenolics might affect the intracellular oxidative system, the changed oxidative balance is able to induce the remodeling of cytoskeletal network from cancer cells.[20] Herein, the remodeling of cytoskeletons is very important for the proliferation, migration, and metastasis of cancer cells.[21] Eventually, the investigation of the change of cytoskeletal network is critical to anticipate the survival of cancer patients. Extending our previous study on the cytoskeletal network for cancer cells,[22] thus, we have focused on the change of cytoskeletal network from cancer cells treated with phenolics-loaded nanocarriers.

2. EXPERIMENTAL DETAILS

2.1. Materials. All the solvents were purchased from Daejung Chemicals (Seoul, Korea). L(+)-Ascorbic acid (Vitamin C), hydroquinone, and sodium periodate were purchased from SAMCHUN CHEMICALS (Seoul, Korea). 10,12-Pentacosadiynoic acid (PCDA), 2-methoxy-4-methyl phenol (Creosol), nordihydroguaiaretic acid (Masoprocol), tannic acid (TA), 2,2-diphenyl-1-picrylhydrazyl (DPPH), tetrabutylammonium hexafluorophosphate, tetra-*n*-butylammonium fluoride (TBAF), propionic acid, triethylsilane, tris-(pentafluorophenyl)borane, silica gel 60 (230−450 mesh), and 3-chloroperoxybenzoic acid were purchased from Alfa Aesar (USA). 4-Methylcatechol, methyl acrylate, 2,4,6-tris(2-pyridyl)-1,3,5-triazine (TPTZ), and ferrocene were purchased from Tokyo Chemical Industry (Tokyo, Japan). Chromium(III) acetonate and eugenol were purchased from Thermo Fisher Scientific (USA). Phenol, pyrogallol, 4-hydroxybenzoic acid, 3,4-dihydroxybenzoic acid, gallic acid, 2,2′-azino-*bis*(3-ethylbenzothiazoline-6-sulfonic acid) diammonium salt (ABTS), and sodium acetate buffer solution were purchased from Sigma-Aldrich (USA). Phosphate-buffered saline (1 × PBS) was purchased from Biosesang (Daejeon, Korea).

2.2. Synthesis of *P$_3$ and *P$_{3-1}$. *P$_3$ was synthesized according to a previous study,[19] and *P$_{3-1}$ was synthetically modified at the last reaction, using propionic acid instead of acrylic acid equivalent, protected eugenol epoxide (10 g, 25.34 mmol, 1.0 equiv), and agitated with hydroquinone (84 mg, 0.76 mmol, 0.03 equiv), propionic acid (3.03 mL, 40.54 mmol, 1.6 equiv), and chromium acetonate (256 mg, 0.76 mmol, 0.03 equiv) for 6 h at 110 °C. After the reaction, the sample was purified with hexane/diethyl ether (7:3) using an auto column (Isolera; Biotage, Sweden). Pure triethylsilane—protected eugenol propionic acid, was obtained. The next step was the same as in our previous study.[19]

2.3. Preparation of TA@PDA. PCDA (0.37 mg, 0.05 mmol) was dissolved in acetone (300 μL). The solution was injected into distilled water (DI water, 20 mL) using a syringe to produce a PCDA assembly suspension in aqueous solution. Subsequently, the suspension was sonicated (P0000VUV; Kodo, Korea) for 1 min and stored for 2 h at 4 °C. The resulting solution was polymerized using a UV lamp (254 nm, 1 mW•cm^{-2}, Vilber, Marne-la-Vallée, France) for 5 min to produce polydiacetylene nano-liposome (PDA). Chitosan (0.125 wt %) was dissolved in DI water (20 mL) with acetic acid (0.4 mL). A mixture of the PDA dispersion in DI water (0.9 mL) and chitosan solution (0.1 mL) was stirred for 2 h at 24 ± 2 °C. The mixed solution was centrifuged (Centurion Scientific, UK) at 15,000 rpm (1411×g) for 15 min to remove unreacted residues and redispersed in DI water (1 mL) to produce a chitosan-PDA nanosome complex (chitosan PDA). Then, TA (0.5 mmol) in DI water (0.5 mL) was added into a chitosan PDA solution and stirred at room temperature for 2 h. After the mixed solution was centrifuged at 15,000 rpm for 15 min, the supernatant was removed and redispersed in DI water (1 mL).

2.4. Antioxidant Activity. The antioxidant activities were measured using DPPH, ABTS, and ferric reducing antioxidant power (FRAP) assays. DPPH solution (100 μL, 100 μM in methanol) and 100 μL of the sample were incubated for 30 min at 24 ± 2 °C. Absorbance was read at 517 nm using a microplate reader (iD5 Multi-Mode Microplate Reader, Molecular Devices, USA). A total of 7 mmol of Trolox-equivalent antioxidant capacity [ABTS, 2,2′-azino-*bis*(3-ethylbenzothiazoline-6-sulfonic acid)] and 2.45 mmol of persulfate dissolved in DI water were incubated for 24 h in the dark at 24 ± 2 °C. To confirm the effect of an oxidant reagent, 0.1 M $NaIO_4$ was added. The ABTS radical solution was diluted to have 0.9 ± 0.1 absorption intensity at 732 nm. ABTS (180 μL) and the sample (20 μL) were then incubated for 10 min to measure the absorbance at 732 nm.

DPPH-scavenging activity and ABTS-scavenging activity were calculated as follows
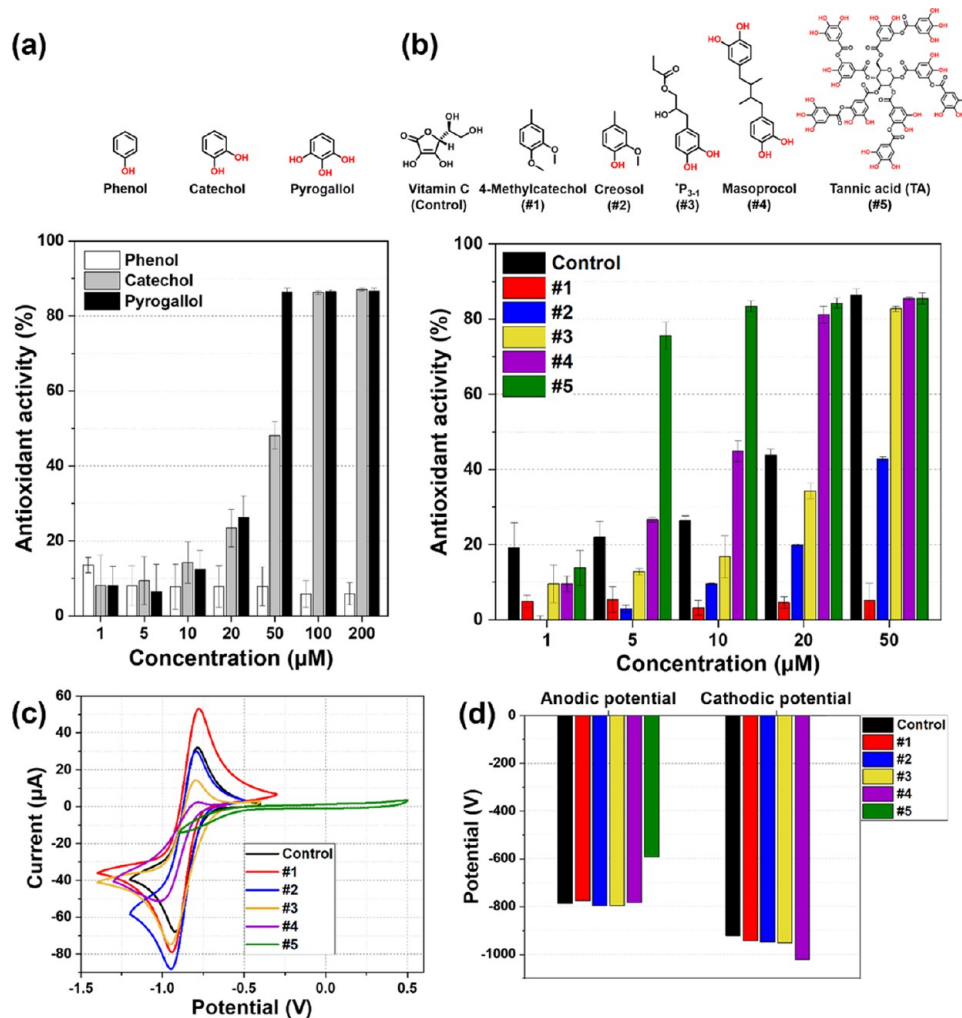
$$\text{antioxidant activity (\%)} = \left(\frac{A_c - A_s}{A_c} \right) \times 100\%$$

A_c is the absorbance of the control (DI water) and DPPH or ABTS solution and A_s is the absorbance of the sample and the DPPH or ABTS solution.

To prepare the ferric reducing/antioxidant power reagent (FRAP) solution, 25 mL of sodium acetate buffer (300 mmol, 10 equiv), 2.5 mL of TPTZ in 40 mmol HCl (1 equiv), and 2.5 mL of FeCl$_3$ (20 mmol, 1 equiv) were incubated for 15 min at 37 °C. The FRAP reagent solution (150 μL) and sample (5 μL) were vortexed (VM-10, DAIHAN Scientific, Korea) and incubated for 30 min at room temperature. The absorption intensity was measured at 594 nm.

FSC$_{50}$ was the concentration required for a 50% free-radical-scavenging activity.

2.5. Electrochemical Measurements. The CV diagram was obtained using a VersaSTAT3 (AMETEK, Berwyn, PA, USA). Glassy carbon was used as the working electrode. Ag/AgCl was used as the reference electrode, and a Pt wire electrode was used as the counter electrode. 0.1 M Tetrabutylammonium hexafluorophosphate and 1.0 mM sample were dissolved in acetonitrile. The scan rate was 0.1 V s^{-1}. To confirm the effect of adding an oxidant reagent, 0.1 M $NaIO_4$

Figure 1. (a) Chemical structures of phenol, catechol, pyrogallol, and their molar concentration-dependent antioxidant activity (%) measured using the DPPH radical-scavenging assay (30 min incubation at 24 ± 2 °C). (b) Chemical structures of (poly)phenolic molecules and their molar concentration-dependent antioxidant activity. The data were expressed as mean $\pm$ standard deviation (SD) (n = 3). (c) CV diagram of (poly)phenolic molecules and (d) oxidation and reduction potential peaks of the (poly)phenolic molecules. CV of 1.0 mM in acetonitrile containing 0.1 M tetrabutylammonium hexafluorophosphate on a glassy carbon working electrode at a scan rate of 0.1 V s^{-1}. *P$_{3-1}$ is a synthetic molecule modified from the literature.[19]

was added to the cells to confirm the effect of the oxidant reagent. All CV accessories were purchased from FRONTIER (Seoul, Korea).

2.6. Characterization of Phenolics and PDA. UV−vis absorption spectra of the phenolics after adding NaIO$_4$ in acetonitrile 5%: D.I water 95% was scanned at wavelengths ranging from 270 to 700 nm. The zeta potential and size of PDA, chitosan PDA, and TA@PDA were measured using a Zetasizer (Zetasizer Nano ZS90, Malvern Panalytical, UK). The morphology and elemental analysis of PDA and TA@PDA was recorded using scanning electron microscopy (SEM) with an energy-dispersive spectrometer.

2.7. Cell Viability Test, Intracellular ROS Assay, and Immunostaining. MDA-MB-231 cells, a human breast cancer cell line, were seeded in a culture medium [phenol-red free RPMI-1640 containing 10% fetal bovine serum (FBS) and 1% antibiotic-antimycotic (AA), GIBCO, USA] in a 96-well plate at a density of 1×10^4 cells per well. The cells were incubated at 37 °C in an atmosphere containing 95% air and 5% CO$_2$. After 24 h, cells were treated with different TA, PDA, and TA@PDA concentrations ranging from 0 to 20 μM (1/5 dilution, PBS containing 20%). After 24 h, the cells were observed using optical microscopy (DMI6000B, LEICA, Germany) and stained with the MTT solution (Sigma-Aldrich, USA) for the cytotoxicity test.

MDA-MB-231 cells were seeded in a 96-well plate at 1×10^4 cells/well density to estimate intracellular ROS levels. After 24 h, the cells were incubated with 20 μM of TA, PDA, or TA@PDA (PBS contained 4%). After 24 h, the cells were washed with 1× buffer solution. DCFDA solution (DCFDA/H2DCFDA—Cellular ROS Assay Kit, Abcam, USA) was diluted with 1× buffer (20 μM) and added to cells, followed by incubation at 37 °C for 45 min. The solution was then removed and transferred to 1× PBS. 2′,7′-Dichlorofluorescein (DCF) fluorescence signals were measured at E_x/E_m = 485/535 nm at the endpoint using the Cytation 1 instrument (Agilent, USA) and BioTek Gen5 software (V3.03, Agilent, USA).

2.8. Immunostaining and Fluorescent Gelatin Degradation Assay. For immunofluorescence imaging, MDA-MB-231 cells were incubated on 15 mm rounded glass coverslips for 24 h, followed by incubation with TA, PDA, and TA@PDA for 24 h. After three washes with 1× DPBS, cells were fixed with 4% paraformaldehyde (PFA) for 30 min at 24 ± 2 °C. The coverslips were incubated in 0.5% Triton X-100 for permeabilization and washed three times. The cells were incubated in a 2% bovine serum albumin (BSA) blocking buffer solution for 30 min and incubated with primary antibodies for 1 h at RT. After three washes with 1× DPBS, fluorescent dye-labeled secondary antibodies were treated to cells and incubated for 30 min at 24 ± 2 °C. Mounted and sealed coverslips on the slides were

visualized using confocal microscopy at 63× objective magnification (LSM700, Carl Zeiss, Germany) and ZEN 3.3 software (blue edition, version 3.3.89.0000, Carl Zeiss, Germany). Colocalization analysis and line profiling were performed using the ImageJ software (version 1.53t, Maryland, USA).

The QCM Gelatin Invadopodia assay Kit was used to investigate invadopodia formation (Merck Millipore, USA). For substrate preparation, coverslips were first coated with dilute poly-L-lysine in deionized water for 20 min at 24 ± 2 °C. After removing poly-L-lysine, the cover glasses were rinsed in triplicates with 1× DPBS. 250 μL of diluted glutaraldehyde in DPBS was added to each well and incubated for 15 min at RT to activate the poly L-lysine surface. Each well was rinsed thrice with 1× DPBS. Fluorescently labeled and unlabeled gelatin were mixed in a 1:5 ratio for gelatin coating. The mixture was added to each well and incubated for 10 min at RT. Each well was rinsed thrice with 1× DPBS. The fluorescent-gelatin substrates were disinfected with 70% ethanol for 30 min at 24 ± 2 °C. After removing and rinsing ethanol with 1× DPBS, 500 μL/well of amino acid-containing growth medium was added to quenching-free aldehydes and incubated for 30 min at 24 ± 2 °C. MDA-MB-231 cells were pretreated with TA, PDA, or TA@PDA for 24 h.

The cells were harvested and seeded in a 4-well plate containing gelatin-coated coverslips at a density of 1.5×10^5 cells per well. Cells were cultured for 24 h and fixed with 4% PFA for 30 min at 24 ± 2 °C. Samples were rinsed in triplicate with staining buffer (DPBS with 2% BSA and 0.25% Triton X-100) for blocking and permeabilization. Fluorescently conjugated phalloidin [tetramethylrhodamine (TRITC)-phalloidin, 2 μg/mL] and DAPI (1 μg/mL) were added and incubated for 1 h at 24 ± 2 °C. The samples were then rinsed with DPBS and mounted on slides. Fluorescent gelatin degradation areas were imaged using confocal microscopy at a 63× objective magnification. Image analysis was performed using ZEN. The diminished fluorescent signals were quantified using ImageJ software.

3. RESULTS AND DISCUSSION

3.1. Interpretation of a Structure−Antioxidant Activity Relationship for Single Phenolic Molecules.
The number of phenolic hydroxyl groups (−OH) is important in antioxidant abilities.[23] For example, gallic acid containing three −OH groups has higher antioxidant activity (FSC_{50} value: 0.92 μg/mL) than caffeic acids with two −OH groups (FSC_{50} value: 3.43 μg/mL).[24] Herein, to systematically investigate the dependency of antioxidant activity on the number of −OH groups within the analogue molecules, phenol (containing one −OH group), catechol (containing two −OH groups), and pyrogallol (containing three −OH groups) were compared using the DPPH radical-scavenging assay (Figure 1a). Phenol showed no noticeable tendency of antioxidant activity according to the concentration, whereas catechol and pyrogallol showed concentration-dependent increases in antioxidant activity in the range of 1−200 μM. Catechol had an antioxidant activity of $48.1 \pm 3.6\%$ at 50 μM and reached $86.3 \pm 0.5\%$ at 100 μM. Pyrogallol attained the highest antioxidant activity of $86.4 \pm 1.0\%$ at 50 μM. The determined FSC_{50} value of phenol cannot be obtained, while those of catechol and pyrogallol were 54 and 30 μM, respectively. Accordingly, the antioxidant activity of the phenolics increased with the number of −OH groups in the phenolic series. To confirm the trend of antioxidant activity depending on the number of −OH groups, the antioxidant activities of another phenolic series (phenolics with different phenolic hydroxyl groups substituted with the same position and one −COOH), 4-hydroxybenzoic acid (4-HBA), 3,4-dihydroxybenzoic acid (3,4-DHBA), and gallic acid (GA) were compared using the DPPH radical-scavenging assay (Figure S1). Similarly, the greater the number of −OH groups in the phenolic series, the

higher antioxidant activity. The FSC_{50} value of 4-HBA could not be determined because of the lack of noticeable antioxidant activity, whereas 3,4-DHBA and GA have 41 and 29 μM of FSC_{50} values, respectively. The phenolic series also confirmed the dependency of the antioxidant activity on the number of phenolic hydroxyl groups.

We further investigated the correlation between the structure of more complex phenolics and antioxidant activity (Figure 1b). Vitamin C (control) is a representative antioxidant component of dietary supplements. The antioxidant activities of five phenolic compounds containing different numbers of −OH groups were evaluated and compared as follows: 4-methylcatechol (#1) has one benzene ring without −OH groups, cresol (#2) has one benzene ring with one −OH group, *P$_{3-1}$ (#3) has one benzene ring with two −OH groups, masoprocol (#4) has two benzene rings with four −OH groups, and tannic acid (TA, #5) has 10 benzene rings with 25 −OH groups. In our previous study, we developed *P$_3$ as a surface primer,[19] and we applied *P$_3$ as an antioxidant because it is a phenol derivative that acts as a free-radical scavenger (Figure S2). Because *P$_3$ has a catechol (two −OH groups) and acrylate group at each molecular end, *P$_{3-1}$ (#3) was synthesized as a molecule with a blocking acrylate group to exclude the potential antioxidant/radical-scavenging effects of the acrylate. Its structure and molecular weight were confirmed using ^{1}H NMR and mass spectrometry, as shown in Figure S2. Hence, the antioxidant activities of *P$_3$, methyl acrylate, and *P$_{3-1}$ were compared (Figure S3). Methyl acrylate did not show antioxidant activity, and the antioxidant activities of *P$_3$ and *P$_{3-1}$ were similar with the same FSC_{50} values of 30 μM. This indicates that the antioxidant activity of *P$_3$ originated from the −OH group and not the acrylate group.

From #2 to #5, the greater the number of −OH groups, the greater the antioxidative activity (the FSC_{50} values of #2, #3, #4, and #5 were determined to be 57, 29, 11, and 3.3 μM, respectively); #1 had no concentration-dependent antioxidant activity. The control (vitamin C) had a FSC_{50} value of 24 μM, and the antioxidant activity originated from the lactone ring with an electron-rich 2-en-2,3-diol-1-one moiety.[25] It can undergo two consecutive one-electron oxidation reactions and the deprotonation of both hydroxyl groups, resulting in the formation of dehydroascorbic acid.[26] Among the experimental groups, #5 showed the strongest antioxidant activity at a range of concentrations (5−50 μM). The ABTS and Frap assays showed the same tendency of antioxidant activity in the experimental groups as shown in the DPPH assay (Figure S4): the antioxidant activity of #5 > #4 > control > #3 > #2.

To compare the oxidation and reduction potentials of the phenolic series, CV diagrams were recorded (Figure 1c). The samples (control, #1, #2, #3, and #4) showed a relatively similar shaped CV diagram, and #5 showed no distinct/very low oxidation and reduction peaks. This suggests that #5 has strong resistance to oxidation, which is consistent with previous studies showing that a lower oxidation peak potential (E_{pa}) shows stronger antioxidant activity.[24,27] As can be seen from the numerical values of the anodic and cathodic potentials in Figure 1d, #5 has the largest oxidation peak, indicating the toughest electrochemical property for oxidation resistance.

Phenolics are readily oxidized by several stimuli, such as oxidants, ozone, and pH changes.[28−30] The phenolics were treated with a strong oxidant ($NaIO_4$) to compare the chemical stability or resistance to the phenolic series'
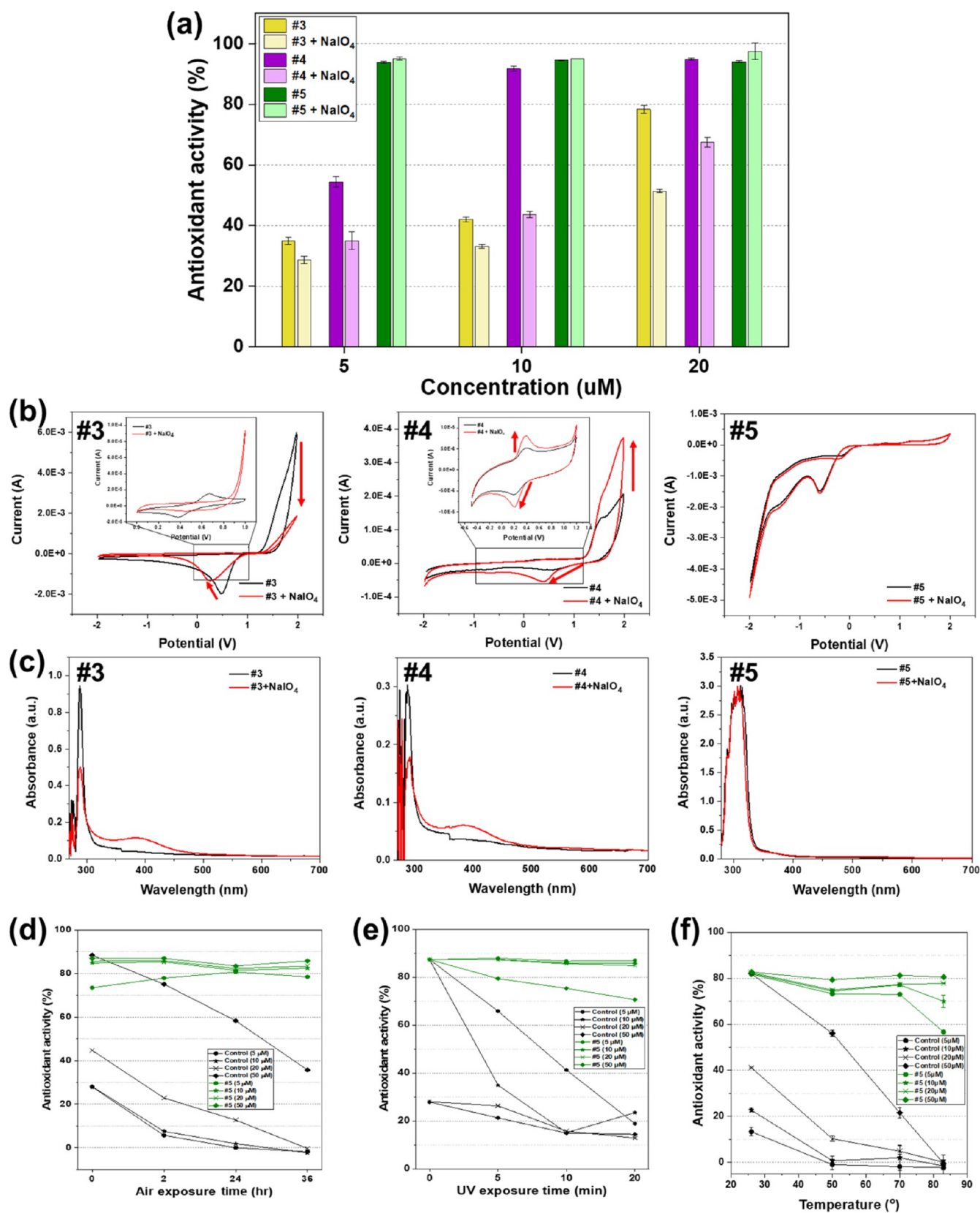
Figure 2. (a) Antioxidant activity measured using the DPPH assay, (b) CV diagram, and (c) UV−vis absorption spectra of phenolic molecules (#3, #4, and #5) after adding NaIO₄ for 30 min incubation at 22 ± 2 °C. Comparison of antioxidant activity between vitamin C (control) and TA (#5) depending on (d) air exposure time, (e) UV (254 nm, 24 Watt) irradiation time, and (f) temperature. The data were expressed as mean ± SD (*n* = 3).
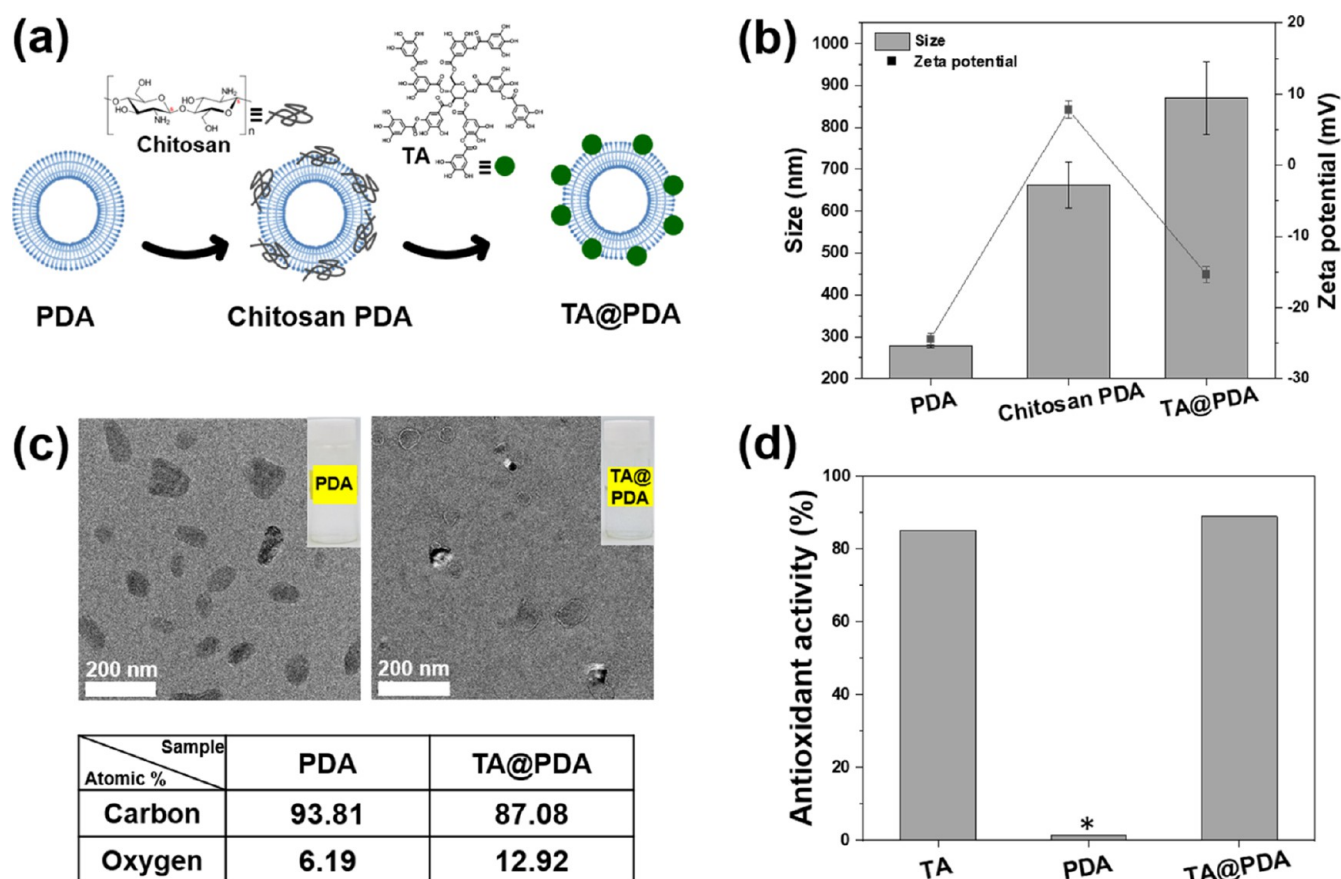
Figure 3. (a) Scheme depicting preparation of TA attracted on polydiacetylene nanocomplexes (TA@PDA). Because the negatively charged TA could not be directly attached to the negatively charged PDA, the PDA nanosomes are coated with chitosan (chitosan PDA). (b) Size and zeta potential of PDA nanosomes, chitosan PDA, and TA@PDA. (c) SEM images with EDS analysis of PDA and TA@PDA to confirm successful complexation with TA containing OH groups. Atomic (carbon and oxygen) percentage (%) of the surface according to the complexation. (inset) Solution sample of PDA nanosomes and TA@PDA. (d) Antioxidant activity of TA, chitosan PDA, and TA@PDA was measured using the DPPH assay (30 min incubation at 24 ± 2 °C). The data were expressed as mean $\pm$ SD ($n = 3$). Statistical analysis was performed using one-way ANOVA (*$p < 0.01$) when compared with TA.

oxidation. Figure 2a−c shows the change in the properties of the phenolic series (#3, #4, and #5) when an oxidized condition is evaluated using DPPH assays, CV diagrams, and UV−vis absorption spectra. When NaIO$_4$ was added to OH groups at 1:1 equiv, the antioxidant activity of #3 and #4 reduced (Figure 2a) significantly in the phenolics. It was reduced by 35% (average value of antioxidant activity from 78.4 to 51.3%) and 29% (average value of antioxidant activity from 94.9 to 67.6%), respectively, under 20 μM of NaIO$_4$ treatment. However, #5 showed no reduction in antioxidant activity at any concentrations of NaIO$_4$ treatment. In addition, there was a change in the CV diagram of #3 and #4 (shift in reduction potential), whereas #5 maintained an unaffected graph (Figure 2b). In both #3 and #4 of UV−vis absorption spectra, the intensity of the phenol peak around 300 nm decreased, and a quinone peak (the oxidized form of phenol, around 400 nm) appeared (Figure 2c). However, no increase or decrease in the peak occurred in sample #5, indicating that the oxidation reaction rarely occurred. We examined the phenolics' CV and UV−vis absorption spectra to monitor the effect of oxidation over a more extended period. The graph for #5 did not change during 0−10 cycles. However, in #3 and #4, the oxidation peak decreased over time. The current in the CV diagram also changed after the addition of NaIO$_4$ (Figure S5a). In UV−vis absorption spectra, the absorption peaks of #3 and

#4 (around 300 nm), corresponding to phenol, immediately decreased after NaIO$_4$ was added, and the absorption peak of quinone (around 400 nm) increased. After 30 min of incubation, the absorption peak at 300 nm decreased, and the absorption peak at approximately 400 nm increased. However, sample #5 showed no change after adding NaIO$_4$ (Figure S5b), indicating that it is strongly resistant to NaIO$_4$-mediated oxidation.

Based on the strongest antioxidant activity and oxidation resistance, #5 (tannic acid) was selected for further studies as an alternative antioxidant to the control (vitamin C). The antioxidant activity of vitamin C is known to be sensitive to external environments, such as air, UV exposure time, and temperature.[31,32] Accordingly, the antioxidant activities of control and #5 were compared under these conditions (Figure 2d−f). In Figure 2d, after 36 h of air exposure, the antioxidant activity of the control was gradually reduced (the average value of antioxidant activity from 88.4 to 35.7% at 50 μM). In contrast, the antioxidant activity of #5 was maintained over 95% of initial activity (the average value of antioxidant activity from 87.1 to 85.8% at 50 μM). In Figure 2e, when UV (254 nm, 24 Watt) was irradiated for 20 min, the antioxidant activity of the control was gradually decreased to less than 20%. However, #5 was preserved with almost the same initial activity in a range of 10−50 μM. In Figure 2f, the antioxidant activity
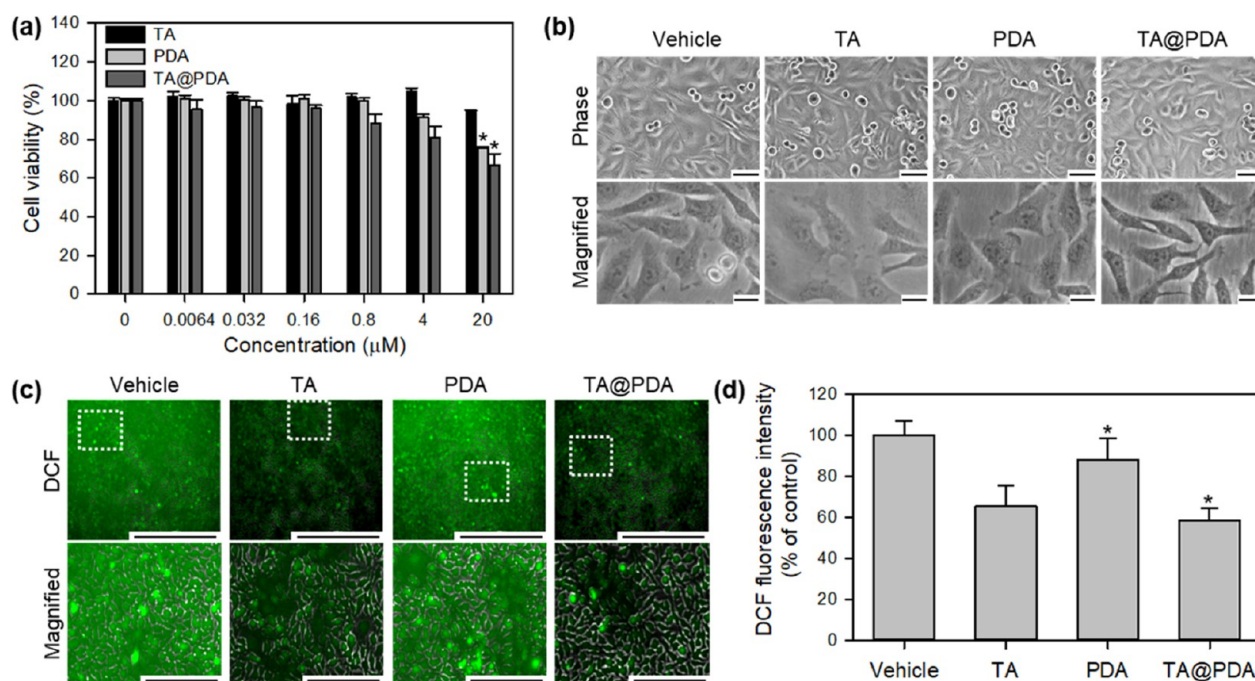
Figure 4. (a) Cell viability graphs and (b) microscopic phase images for MDA-MB-231 cells treated with TA, PDA, and TA @PDA, respectively (Scale bars = 50 and 20 μm in magnified images). (c) Fluorescence microscopic images for the cancer cells incubated with each condition were depicted for 24 h using the Cytation 1 Cell Imaging Multi-Mode Reader, the scale represents 1 mm. The white dotted box inset in the upper image is magnified and shown at higher magnification in the bottom panel (Scale bars = 250 μm). (d) Measured DCF fluorescence intensities measured from (c) analyzed using the Gen5 software. Data represent means ± SD (n = 4). Statistical analysis was performed using one-way ANOVA (*$p <$ 0.01) when compared with TA (20 μM).

of the control was decreased at above 50 °C. All the antioxidant activity was lost at 83 °C, while #5 nearly maintained its antioxidant activity even at 83 °C. In summary, #5 had a higher antioxidant activity stability under various environmental conditions than the control.

As supplementary treatment molecules for antioxidant functionality, phenolic compounds have been used as anticancer drug-delivery carriers.[16,33] Epigallocatechin-3-O-gallate (EGCG), a natural polyphenol, has been combined with the anticancer drug doxorubicin, improving its therapeutic effect.[33] EGCG could protect the expression of carbonyl reductase 1 protein and inhibit doxorubicinol generation of doxorubicin, reducing cardiac toxicity and doxorubicin-mediated toxicity. TA is a relatively bulk molecule among natural polyphenolics—making it difficult to perform cellular uptake; however, nanoparticles, such as polydiacetylene nano-liposome (PDA), could show cell endocytosis and exhibit potential as drug carrier platforms in our previous study.[34] Hence, we would like to apply TA as surface treatment materials, with one of the loading approaches, onto PDA nanocarriers for antioxidation-functionalized drug delivery. Because the negatively charged TA (#5) could not be directly attached to the negatively charged PDA, TA was treated with electrostatic attraction after chitosan coating (chitosan PDA) (Figure 3a). After chitosan treatment, the size of the chitosan PDA increased to 660 ± 60 nm. After TA treatment (TA@ PDA), the size increased to 870 ± 90 nm. After chitosan treatment on PDA with −24.4 ± 0.8 mV zeta potential, it had a positive charge of 7.8 ± 1.2 mV and after TA treatment, it had a negative charge of −15.4 ± 1.1 mV (Figure 3b). As shown in Figure 3c, the oxygen ratio on the surface of TA@PDA (12.92%) was higher than that of PDA (6.19%), indicating successful complexation with TA-containing OH groups.

While PDA had no noticeable antioxidant activity, TA@PDA exhibited 85% antioxidant activity of initial-treated TA (Figure 3d).

3.2. Antioxidative Impact of Phenolic Surface Treatment on Cancer Cell Behaviors. The antioxidant potential of the prepared TA@PDA for cancer cells was evaluated by investigating cellular viability, morphological changes, and antioxidant activity. First, serially diluted TA@PDA was treated with the cultivated MDA-MB-231 cells, and the cellular viability was investigated by the MTT assay (Figure 4a). The measured values were compared to those for free TA and PDA as controls. As shown in Figures 2 and 4a, TA possesses sufficient antioxidant activity under the cellular survival region up to 20 μM. Thus, there was no critical inhibition of cellular proliferation with 20 μM free TA. However, TA@PDA exhibited reduced cell viability compared to free TA or PDA. Although treatment with PDA reduced the viability of cancer cells, statistical significance for the treatment with TA@PDA was confirmed ($p = 0.008$). We would like to find a certain concentration that could contain enough antioxidant activity, while showing different cellular viability and cellular behavior—experimental concentration of TA at 20 μM was appropriate for further studies. As shown in Figure 4b, cellular morphology was altered, and the cellular area was spread after treatment with TA (20 μM). Otherwise, the cancer cells treated with TA@PDA were minutely diminished, and the dividing cell counts were reduced.

The cellular antioxidant activity of TA loaded from TA@ PDA was evaluated using a dichlorodihydrofluorescein diacetate (DCF-DA) assay. When the fluorogenic probe DCF-DA was used, the fluorescent green light from the interrogating cells might be exhibited because of the transformation into DCF from DCF-DA through the oxygen-
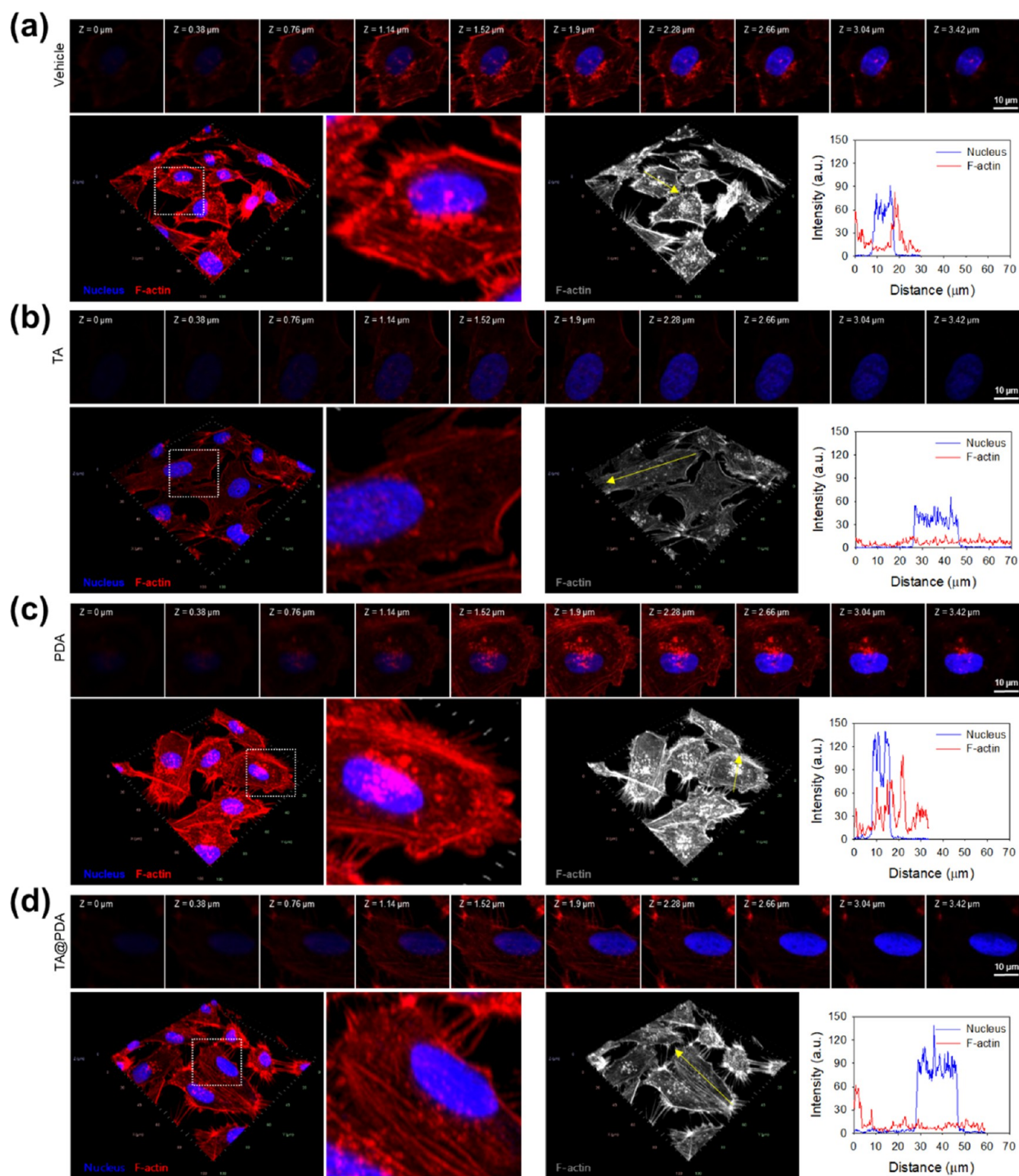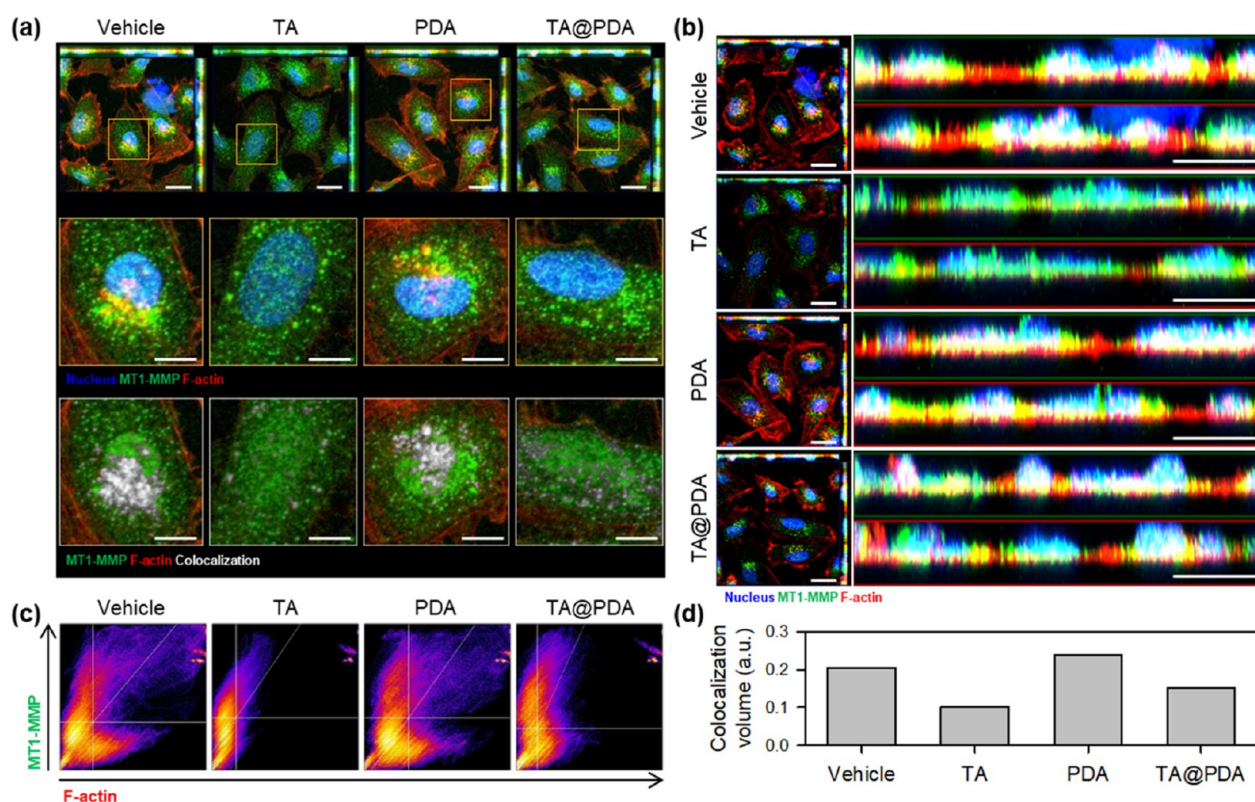
Figure 5. Confocal microscopic images for analyzing the F-actin-based cytoskeletal network of MDA-MD-231 cells treated with (a) vehicle control, (b) TA, (c) PDA, and (d) TA-PDA. Representative Z-stack images were acquired from the bottom to the top of the cells (Scale bars = 10 μm). The white dashed box in the 2.5D images was magnified for actin distribution analysis. The histogram shows the actin filament strength in the section indicated by the yellow arrow. Nucleus was stained with Hoechst33342 (blue), and the histogram graph's blue lines indicate fluorescence signal intensity profiles.

ation process by intracellular ROS. In the magnified fluorescence microscopic images, green-fluorescent cells were remarkably reduced after treatment with TA or TA@PDA (Figure 4c). As depicted in Figure 4d, TA-treated cells (free

TA or TA@PDA) exhibited decreased fluorescence signal intensities compared to the vehicle control. These results demonstrate that the loaded TA from TA@PDA affected cellular viability and antioxidant activity.

H

Figure 6. (a) Confocal microscopy for colocalization analysis and (b) orthogonal projections of MT1-MMP (green) and F-actin (red) from maximum intensity projection images (Scale bars = 20 μm). Colocalization was evaluated in ROIs (orange line box, scale bars = 10 μm in magnified images) using colocalization analysis plugins by ImageJ. (c) 2D scatterplot for MT1-MMP (y-axis) and F-actin (x-axis) colocalization visualized using the calculated thresholds determined for each color channel. (d) Bar chart represents the percentage of voxels which have both MT1-MMP and F-actin intensities above threshold in (c). The number of pixels in the scatterplot's quadrant I area was divided by the total number of pixels in the scatterplot.

Thus, we hypothesized that TA-induced cytoskeletal remodeling of cancer cells is related to their proliferation and invasiveness. Changes in the cytoskeletal network are critical to anticipate cellular migration potential. Cytoskeleton remodeling is a crucial process in cellular elongation and contractility. Intracellular ROS are important for modulating actin polymerization dynamics.[35] Intracellular ROS oxidizes actin. In particular, Cys374 from the C-terminal region of β-actin can be oxidized to form both G-actin (monomeric) and F-actin (polymerized)[36] when the oxidized forms of actin increase, actin polymerization is reduced because of intracellular ROS. Intracellular actin is evenly distributed in the migration direction, and cellular polarity is induced by actin polymerization for ruffling and the formation of lamellipodia.[35] In lamellipodium, the increase in actin networking is related to the development of traction force, which is affected by cellular migration. Herein, we examined whether the antioxidant activity of the loaded TA at TA@PDA was involved in cellular migration capability by analyzing the cytoskeleton distribution and its network.

As shown in Figure 5a, a strong intensity from actin was observed in needle-like filopodia and lamellipodia from vehicle-treated cancer cells. Moreover, z-stacked confocal microscopic images demonstrated a dot-like structure of distributed actin at the perinuclear region of the ventral cell surface (Figure 5c). After treatment with PDA, results similar to those of vehicle-control cells were obtained. A dot-like structure was exhibited without TA. After treatment of cancer cells with TA or PDA@TA, the fluorescent actin intensity was

remarkably reduced at both the cellular periphery and cytosol, and an actin-rich structure was not observed near the nucleus. From byline profiling of the representative cells, as shown in Figure 5, the analysis graphs for the fluorescence intensity from the nucleus and actin coincided with the observed results. Interestingly, the dot-like structure of actins in the perinuclear region appeared transiently. A specific short protrusion form is the podosome.

Podosomes are transient cell surface structures and one of the important actin structures within the cell.[37,38] These small protrusions, appearing on the ventral cell surface, play a crucial role in the cell's interaction with the surrounding environment and participate in physiological and pathological processes, such as tissue remodeling and inflammatory responses. Furthermore, podosomes, characterized by their presence in metastatic cancer cells, serve as a recruitment for enzymes, including metalloproteinases, which induce the degradation of the surrounding substrates.[39,40]

The process of degrading matrix components through proteolytic activity influences biological processes, such as cell motility, invasion, and differentiation. Therefore, the functions and roles of podosomes are implicated in various physiological processes, including cancer development and metastasis, as well as inflammatory diseases. Hence, we investigated the structural characteristics of the intracellular actin structures based on the treatment with TA. In Figure 5, the analysis of z-stack images of F-actin revealed the presence of dot-like structures (podosomes) in the ventral surface region, corresponding to the area above the nucleus. However,
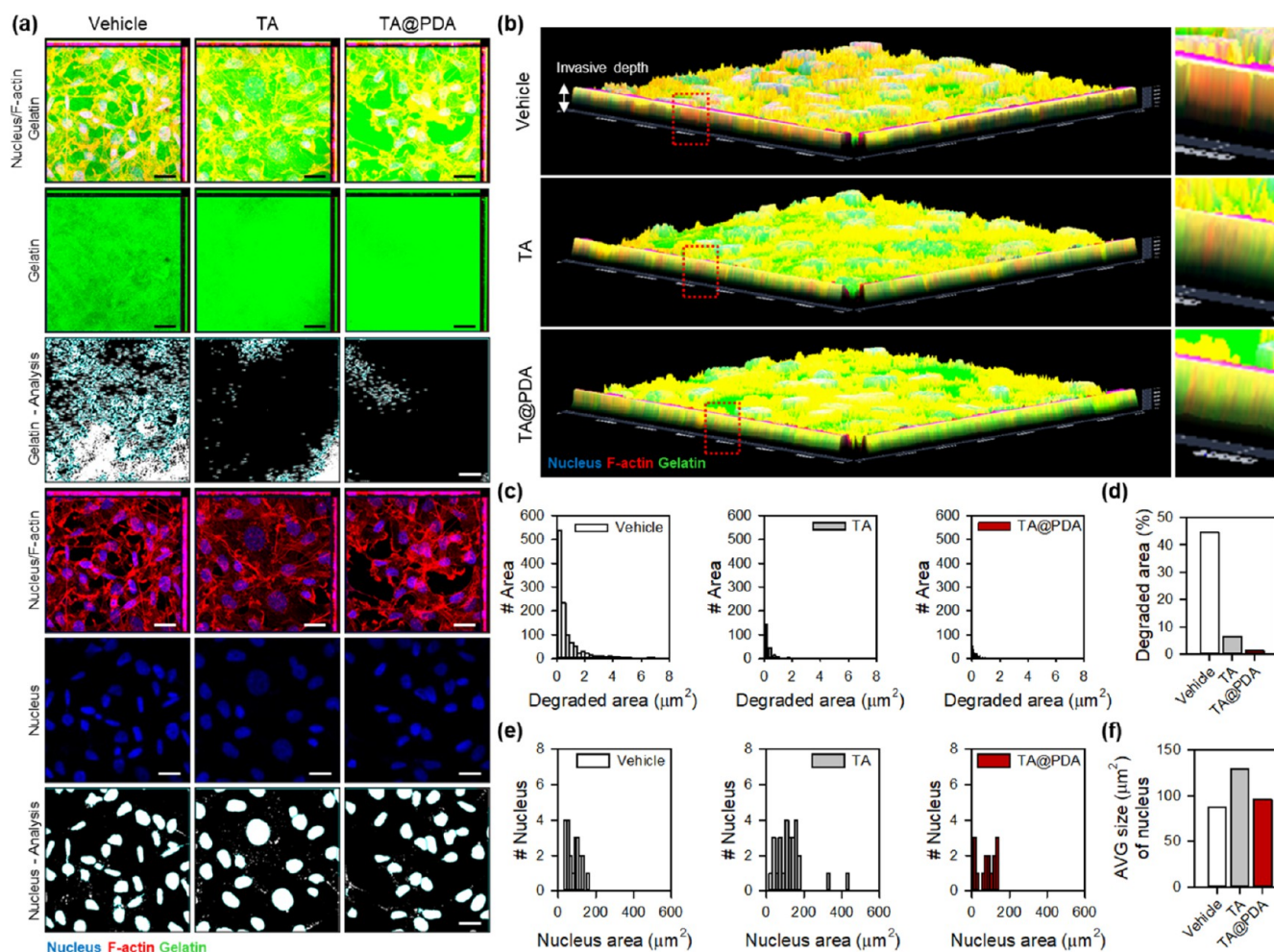
Figure 7. (a) Fluorescein-labeled gelatin matrix (green) degradation with invadopodia-related puncta (black area) by each cell treated with the vehicle, TA, or TA@PDA. Actin structures (red) and nucleus (blue) were stained with TRITC-phalloidin and Hoechst33342 (scale bars = 20 μm). In the third and sixth columns, analyzed images obtained from the "analyze particles" function of the ImageJ program to measure the gelatin degradation area and nucleus area. (b) Red fluorescent actin structures present the gelatin-penetration depth visualized in an orthogonal view. (c) Histograms for the distribution of the degradation area and (d) graph for the percentage of degradation area. (e) Histogram for the distribution of the nucleus area and (f) graph for the average nuclear area based on histography analysis.

podosomes disappeared under TA-treated conditions (TA, TA@PDA), indicating structural changes in actin that may be associated with cellular transition and invasive potential. To confirm our findings, we conducted a colocalization analysis between actin structures regarded to be podosomes and MT1-MMP, a biomarker for invasive potential, as shown in Figure 6. Additionally, we verified the matrix degradation ability, such as gelatin degradation, to demonstrate the correlation between podosome formation, cell−matrix interaction, and cellular invasive function, as shown in Figure 7.

MT1-MMP is expressed in invasive cancer cells, exhibiting the potential for migration and invasion. In particular, aggressive breast cancer MDA-MB-231 cells highly express MT1-MMP. MT1-MMP is a critical biomarker for controlling and blocking the metastasis of cancer cells because of its ability to degrade the surrounding substrates and extracellular matrix (ECM) by colocalization with actin in the moving area.[41−43] Therefore, multicolor labeling confocal microscopy of cancer cells treated with TA@PDA was conducted to analyze the colocalization between MT1-MMP and F-actin. In addition, the orthogonal view was investigated. Figure 6a depicts podosome formation (red spots) in the perinuclear region

and colocalized with MT1-MMP (green dots) in both vehicle- and PDA-treated conditions. A positive correlation between podosomes and MT1-MMP was confirmed in further processing, and the overlapped area was converted to a gray color (Figure 6a, third column). In the vehicle- and PDA-treated groups, gray-colored colocalization between podosomes and MT1-MMP was observed at the perinuclear site. Colocalization between podosomes and MT1-MMP was reduced in both TA and TA@PDA. In addition, the maximum intensity projection for the lateral confocal microscopic images was confirmed (Figure 6b). Without TA treatment, yellow dotted areas due to an overlap between podosomes and MT1-MMP were observed from an orthogonal view. Furthermore, a colocalization volume graph is depicted from each orthogonal view (Figure 6c,d). After treatment with TA@PDA, the colocalization between the podosomes and MT1-MMP was diminished.

A gelatin-based invasion assay was conducted to verify further the antioxidant potential of TA-loaded PDA (TA@ PDA) in inhibiting cellular invasiveness. After treatment with TA@PDA, the gelatin degradation area, nucleus size, and morphology of the invadopodia were investigated for

comprehensively analyzing the metastatic potential of cancer cells. As shown in Figure 7a, the degraded gelatin area for the vehicle treatment condition was larger than other results obtained from TA-containing conditions. Orthogonal (2.5D) confocal microscopy images were reconstructed from the maximum intensity projection (Figure 7b). From a magnification view, the frequency of protruded F-actin (red) toward the gelatin region (green) was increased and the invasion depth was deeper without TA-containing PDA. In the case of free TA-treatment, protruding F-actin was observed in the gelatin region. However, the invasive depth was reduced compared to the vehicle-treatment condition. In particular, TA@PDA remarkably reduced the invasion depth and diminished the protruding F-actin. An identical tendency was confirmed by the quantification of the gelatin degradation area using further image processing (Figure 7c). In the TA@PDA treatment conditions, statistical analysis of the degraded gelatin area confirmed a meaningfully reduced distribution. The degraded area by the vehicle-treated cells was 44.6%, which was 35 times larger than the degraded area by TA@PDA-treated cells (Figure 7d). On the other hand, after treatment with free TA, polyploid giant cancer cells and an expanded nucleus area were observed due to mitotic damage (Figures 5 and 7a). TA is an antioxidant that arrests the G1/S phase in various cancer cells.[37,44] Moreover, actin polymerization and the tubulin network were inhibited by TA treatment. During mitosis, newly synthesized actin can exist in the nucleus because of the complexing between cytoplasmic and nucleoplasmic pools. During the early G1 phase, actin in the intranucleus region is assembled, expanding the nucleus by generating protrusions during nuclear enveloping.[44,45] In a normal state, nuclear actin filaments are degraded in the G1 phase to maintain the F-actin network dynamics for the progression of the cell cycle. In our results, free TA-treated cancer cells exhibited a reduction in cytoskeletal formation that affected the cell cycle process and expansion of the nucleus area. Based on image analysis, the average nucleus size from the experimental cells was estimated, and the changed distribution was confirmed (Figure 7e). As expected, the nucleus size of TA@PDA-treated cells was much larger than that of vehicle-treated cells. It owes the releasing of the loaded TA from TA@PDA (Figure 7f). In the TA@PDA-treated condition, however, the narrow distribution of the nucleus area and small average nucleus area were confirmed compared to the free TA-treated conditions. These results demonstrate the effective formulation of TA@PDA for the localized release of TA in the cytoplasmic region. In terms of endocytosis ability of PDA nanocarriers, TA@PDA was more effective in controlling the metastatic potential of cancer cells than free TA without a critical change in the nucleus size. Abnormally generated polyploid giant cancer cells with large nuclei have the potential for tumor recurrence.[40,45]

4. CONCLUSIONS

The antioxidant activity of single phenolics was compared based on the number of phenolic hydroxyl groups in the phenolics. The strongest antioxidative TA with the highest number of groups was stable under air exposure, UV light irradiation, and temperature variation compared to vitamin C as a representative antioxidant. Furthermore, TA was loaded onto the drug delivery carriers for antioxidant functionalization. The formulated TA@PDA reduced MT1-MMP levels in cancer cells and effectively diminished the invasive potential of

cancer cells due to the change of cytoskeletal network. The natural phenolic molecules, TA, could be utilized as a surface treating molecule of drug delivery carriers toward diverse diseases requiring antioxidation functionalization.

■ ASSOCIATED CONTENT

ⓈI Supporting Information

The Supporting Information is available free of charge at https://pubs.acs.org/doi/10.1021/acsami.3c04693.

Chemical structures of 4-HBA, 3,4-DHBA, GA; molar concentration-dependent antioxidant activity measured by the DPPH assay; ^{1}H NMR and mass spectra of synthetic molecules; antioxidant activity of phenolic molecules measured by ABTS and FRAP assay; and the CV diagram depicting changes in phenolic molecules over time (PDF)

■ AUTHOR INFORMATION

Corresponding Authors

Jaemoon Yang − Department of Radiology, College of Medicine, Seoul 03722, Republic of Korea; Systems Molecular Radiology, Yonsei University, Seoul 03722, Republic of Korea; Convergence Research Center for Systems Molecular Radiological Science, Yonsei University, Seoul 03722, Republic of Korea; Email: 177hum@yuhs.ac

Sungbaek Seo − Department of Biomaterials Science (BK21 FOUR Program), College of Natural Resources and Life Science/Life and Industry Convergence Research Institute, Pusan National University, Miryang 50463, Republic of Korea; ⓞ orcid.org/0000-0001-5813-4616; Email: sbseo81@pusan.ac.kr

Authors

Jaewon Jung − Department of Biomaterials Science (BK21 FOUR Program), College of Natural Resources and Life Science/Life and Industry Convergence Research Institute, Pusan National University, Miryang 50463, Republic of Korea

Minhee Ku − Department of Radiology, College of Medicine, Seoul 03722, Republic of Korea; Systems Molecular Radiology, Yonsei University, Seoul 03722, Republic of Korea; Convergence Research Center for Systems Molecular Radiological Science, Yonsei University, Seoul 03722, Republic of Korea

Suhui Jeong − Department of Biomaterials Science (BK21 FOUR Program), College of Natural Resources and Life Science/Life and Industry Convergence Research Institute, Pusan National University, Miryang 50463, Republic of Korea

Nara Yoon − Department of Radiology, College of Medicine, Seoul 03722, Republic of Korea; Systems Molecular Radiology, Yonsei University, Seoul 03722, Republic of Korea; Convergence Research Center for Systems Molecular Radiological Science, Yonsei University, Seoul 03722, Republic of Korea

Jae Hyun Park − Young Chemical Co. Ltd., Gimhae 50969, Republic of Korea

Han Sung Youn − Young Chemical Co. Ltd., Gimhae 50969, Republic of Korea

Complete contact information is available at:
https://pubs.acs.org/10.1021/acsami.3c04693

Author Contributions

#J.J., M.K., and S.J. contributed equally to this work.

■ REFERENCES

(1) Panzella, L.; Napolitano, A. Natural Phenol Polymers: Recent Advances in Food and Health Applications. *Antioxidants* **2017**, *6*, 30.

(2) Kiokias, S.; Oreopoulou, V. A Review of the Health Protective Effects of Phenolic Acids against a Range of Severe Pathologic Conditions (Including Coronavirus-Based Infections). *Molecules* **2021**, *26*, 5405.

(3) Balasundram, N.; Sundram, K.; Samman, S. Phenolic Compounds in Plants and Agri-industrial by-Products: Antioxidant Activity, Occurrence, and Potential Uses. *Food Chem.* **2006**, *99*, 191−203.

(4) Bjørklund, G.; Dadar, M.; Martins, N.; Chirumbolo, S.; Goh, B. H.; Smetanina, K.; Lysiuk, R. Brief Challenges on Medicinal Plants: An Eye-Opening Look at Ageing-Related Disorders. *Basic Clin. Pharmacol. Toxicol.* **2018**, *122*, 539−558.

(5) Shon, M.-S.; Lee, Y.; Song, J.-H.; Park, T.; Lee, J. K.; Kim, M.; Park, E.; Kim, G.-N. Anti-aging Potential of Extracts Prepared from Fruits and Medicinal Herbs Cultivated in the Gyeongnam Area of Korea. *Prev. Nutr. Food Sci.* **2014**, *19*, 178−186.

(6) Vuolo, M. M.; Lima, V. S.; Maróstica Junior, M. R. Phenolic Compounds. In *Bioactive Compounds*; Elsevier, 2019, pp 33−50.

(7) Salehi, B.; Mishra, A. P.; Nigam, M.; Sener, B.; Kilic, M.; Sharifi-Rad, M.; Fokou, P. V. T.; Martins, N.; Sharifi-Rad, J. Resveratrol: A Double-Edged Sword in Health Benefits. *Biomedicines* **2018**, *6*, 91.

(8) Ayoub, M.; de Camargo, A. C.; Shahidi, F. Antioxidants and Bioactivities of Free, Esterified and Insoluble-bound Phenolics from Berry Seed Meals. *Food Chem.* **2016**, *197*, 221−232.

(9) Rahman, M.; Rahaman, S.; Islam, R.; Rahman, F.; Mithi, F. M.; Alqahtani, T.; Almikhlafi, M. A.; Alghamdi, S. Q.; Alruwaili, A. S.; Hossain, S.; et al. Role of Phenolic Compounds in Human Disease: Current Knowledge and Future Prospects. *Molecules* **2021**, *27*, 233.

(10) Anantharaju, P. G.; Gowda, P. C.; Vimalambike, M. G.; Madhunapantula, S. V. An Overview on the Role of Dietary Phenolics for the Treatment of Cancers. *Nutr. J.* **2016**, *15*, 99.

(11) Lobo, V.; Patil, A.; Phatak, A.; Chandra, N. Free Radicals, Antioxidants and Functional Foods: Impact on Human Health. *Pharmacogn. Rev.* **2010**, *4*, 118.

(12) Rigoussen, A.; Verge, P.; Raquez, J.-M.; Dubois, P. Natural Phenolic Antioxidants As a Source of Biocompatibilizers for Immiscible Polymer Blends. *ACS Sustain. Chem. Eng.* **2018**, *6*, 13349−13357.

(13) Pospíšil, J. Mechanistic action of Phenolic Antioxidants in Polymers—A review. *Polym. Degrad. Stab.* **1988**, *20*, 181−202.

(14) Weng, X. C.; Huang, Y. Relationship Structure-Antioxidant Activity of Hindered Phenolic Compounds. *Grasas Aceites* **2014**, *65*, No. e051.

(15) Birben, E.; Sahiner, U. M.; Sackesen, C.; Erzurum, S.; Kalayci, O. Oxidative Stress and Antioxidant Defense. *World Allergy Organ. J.* **2012**, *5*, 9−19.

(16) Yi, Z.; Chen, G.; Chen, X.; Ma, X.; Cui, X.; Sun, Z.; Su, W.; Li, X. Preparation of Strong Antioxidative, Therapeutic Nanoparticles Based on Amino Acid-Induced Ultrafast Assembly of Tea Polyphenols. *ACS Appl. Mater. Interfaces* **2020**, *12*, 33550−33563.

(17) Chen, X.; Yi, Z.; Chen, G.; Ma, X.; Su, W.; Deng, Z.; Ma, L.; Tong, Q.; Ran, Y.; Li, X. Carrier-Enhanced Photodynamic Cancer Therapy of Self-Assembled Green Tea Polyphenol-Based Nanoformulations. *ACS Sustain. Chem. Eng.* **2020**, *8*, 16372−16384.

(18) Shan, L.; Fan, W.; Wang, W.; Tang, W.; Yang, Z.; Wang, Z.; Liu, Y.; Shen, Z.; Dai, Y.; Cheng, S.; et al. Organosilica-Based Hollow Mesoporous Bilirubin Nanoparticles for Antioxidation-Activated Self-Protection and Tumor-Specific Deoxygenation-Driven Synergistic Therapy. *ACS Nano* **2019**, *13*, 8903−8916.

(19) Seo, S.; Lee, D. W.; Ahn, J. S.; Cunha, K.; Filippidi, E.; Ju, S. W.; Shin, E.; Kim, B.-S.; Levine, Z. A.; Lins, R. D.; et al. Significant Performance Enhancement of Polymer Resins by Bioinspired Dynamic Bonding. *Adv. Mater.* **2017**, *29*, 1703026.

(20) Balta, E.; Kramer, J.; Samstag, Y. Redox Regulation of the Actin Cytoskeleton in Cell Migration and Adhesion : On the Way to a Spatiotemporal View. *Front Cell Dev Biol.* **2021**, *8*, 1−11.

(21) Li, X.; Wang, J. Mechanical Tumor Microenvironment and Transduction : Cytoskeleton Mediates Cancer Cell Invasion and Metastasis. *Int J Biol Sci* **2020**, *16*, 2014−2028.

(22) Ku, M.; Kim, H.-J.; Yau, S. Y.; Yoon, N.; Kim, N. H.; Yook, J. I.; Suh, J.-S.; Kim, D.-E.; Yang, J. Microsphere-Based Nanoindentation for the Monitoring of Cellular Cortical Stiffness Regulated by MT1-MMP. *Small* **2018**, *14*, 1803000.

(23) Zeb, A. Concept, Mechanism, and Applications of Phenolic Antioxidants in Foods. *J. Food Biochem.* **2020**, *44*, No. e13394.

(24) Li, X.; Gao, Y.; Xiong, H.; Yang, Z. The Electrochemical Redox Mechanism and Antioxidant Activity of Polyphenolic Compounds based on Inlaid Multi-walled Carbon Nanotubes-modified Graphite Electrode. *ChemistryOpen* **2021**, *19*, 961−973.

(25) Pehlivan, F. E. Vitamin C: An Antioxidant Agent. *Vitamin C*; Intech: 2017; pp 23−35.

(26) Macan, A. M.; Kraljević, T. G.; Raić-malić, S. Therapeutic Perspective of Vitamin C and its Derivatives. *Antioxidants* **2019**, *8*, 247.

(27) Steven, J. T.; Golovko, V. B.; Johannessen, B.; Marshall, A. T. Electrochemical Stability of Carbon-supported Gold Nanoparticles in Acidic Electrolyte during Cyclic Voltammetry. *Electrochim. Acta* **2016**, *187*, 593−604.

(28) Rana, M. S.; Guzman, M. I. Oxidation of Phenolic Aldehydes by Ozone and Hydroxyl Radicals at the Air−Water Interface. *J. Phys. Chem. A* **2020**, *124*, 8822−8833.

(29) Mirshafian, R.; Wei, W.; Israelachvili, J. N.; Waite, J. H. α β-Dehydro-Dopa: A Hidden Participant in Mussel Adhesion. *Biochemistry* **2016**, *55*, 743−750.

(30) Ryu, J. H.; Messersmith, P. B.; Lee, H. Polydopamine Surface Chemistry: A Decade of Discovery. *ACS Appl. Mater. Interfaces* **2018**, *10*, 7523−7540.

(31) Michels, A. J.; Frei, B. Myths, Artifacts, and Fatal Flaws: Identifying Limitations and Opportunities in Vitamin C Research. *Nutrients* **2013**, *5*, 5161−5192.

(32) Lykkesfeldt, J.; Poulsen, H. E. Is Vitamin C Supplementation Beneficial? Lessons Learned from Randomised Controlled Trials. *Br. J. Nutr.* **2010**, *103*, 1251−1259.

(33) Shan, L.; Gao, G.; Wang, W.; Tang, W.; Wang, Z.; Yang, Z.; Fan, W.; Zhu, G.; Zhai, K.; Jacobson, O.; et al. Self-assembled Green Tea Polyphenol-based Coordination Nanomaterials to Improve Chemotherapy Efficacy by Inhibition of Carbonyl Reductase 1. *Biomaterials* **2019**, *210*, 62−69.

(34) Park, K. H.; Ku, M.; Yoon, N.; Hwang, D. Y.; Lee, J.; Yang, J.; Seo, S. Effect of Polydiacetylene-based Nanosomes on Cell Viability and Endocytosis. *Nanotechnology* **2019**, *30*, 245101.

(35) Ishimoto, T.; Mori, H. Control of Actin Polymerization via Reactive Oxygen Species Generation using Light or Radiation. *Front. Cell Dev. Biol.* **2022**, *10*, 10.

(36) Meng, Z.; Li, Z.; Xie, M.; Yu, H.; Jiang, L.; Yao, X. TM9SF4 is an F-actin Disassembly Factor that Promotes Tumor Progression and Metastasis. *Nat. Commun.* **2022**, *13*, 5728.

(37) Darvin, P.; Baeg, S. J.; Joung, Y. H.; Sp, N.; Kang, D. Y.; Byun, H. J.; Park, J. U.; Yang, Y. M. Tannic Acid Inhibits the Jak2/STAT3 Pathway and Induces G1/S Arrest and Mitochondrial Apoptosis in YD-38 Gingival Cancer Cells. *Int. J. Oncol.* **2015**, *47*, 1111−1120.

(38) Murphy, D. A.; Courtneidge, S. A. The "ins" and "outs" of Podosomes and Invadopodia: Characteristics, Formation and Function. *Nat. Rev. Mol. Cell Biol.* **2011**, *12*, 413−426.

(39) Flynn, D. C.; Cho, Y.; Vincent, D.; Cunnick, J. M. Podosomes and Invadopodia: Related structures with Common Protein Components that May Promote Breast Cancer Cellular Invasion. *Breast Cancer Basic Clin. Res.* **2008**, *2*, BCBCR.S789.

(40) Hoshino, D.; Branch, K. M.; Weaver, A. M. Signaling Inputs to Invadopodia and Podosomes. *J. Cell Sci.* **2013**, *126*, 2979−2989.

(41) Ferrari, R.; Martin, G.; Tagit, O.; Guichard, A.; Cambi, A.; Voituriez, R.; Vassilopoulos, S.; Chavrier, P. MT1-MMP Directs Force-producing Proteolytic Contacts that Drive Tumor Cell Invasion. *Nat. Commun.* **2019**, *10*, 4886.

(42) Jiang, W. G.; Davies, G.; Martin, T. A.; Parr, C.; Watkins, G.; Mason, M. D.; Mansel, R. E. Expression of Membrane Type-1 Matrix Metalloproteinase, MT1-MMP in Human Breast Cancer and its Impact on Invasiveness of Breast Cancer Cells. *Int. J. Mol. Med.* **2006**, *17*, 583−590.

(43) Rossé, C.; Lodillinsky, C.; Fuhrmann, L.; Nourieh, M.; Monteiro, P.; Irondelle, M.; Lagoutte, E.; Vacher, S.; Waharte, F.; Paul-Gilloteaux, P.; et al. Control of MT1-MMP Transport by Atypical PKC during Breast-cancer Progression. *Proc. Natl. Acad. Sci. U.S.A.* **2014**, *111*, E1872−E1879.

(44) Moore, H. M.; Vartiainen, M. K. F-actin Organizes the Nucleus. *Nat. Cell Biol.* **2017**, *19*, 1386−1388.

(45) Zhou, X.; Zhou, M.; Zheng, M.; Tian, S.; Yang, X.; Ning, Y.; Li, Y.; Zhang, S. Polyploid Giant Cancer Cells and Cancer Progression. *Front. Cell Dev. Biol.* **2022**, *10*, 10.